



This is a repository copy of *Assessment of semi-mechanistic bubble departure diameter modelling for the CFD simulation of boiling flows*.

White Rose Research Online URL for this paper:
<https://eprints.whiterose.ac.uk/186587/>

Version: Accepted Version

Article:

Colombo, M. orcid.org/0000-0002-4335-4250, Thakrar, R., Fairweather, M. et al. (1 more author) (2019) Assessment of semi-mechanistic bubble departure diameter modelling for the CFD simulation of boiling flows. *Nuclear Engineering and Design*, 344. pp. 15-27. ISSN 0029-5493

<https://doi.org/10.1016/j.nucengdes.2019.01.014>

© 2019 Elsevier B.V. This is an author produced version of a paper subsequently published in *Nuclear Engineering and Design*. Uploaded in accordance with the publisher's self-archiving policy. Article available under the terms of the CC-BY-NC-ND licence (<https://creativecommons.org/licenses/by-nc-nd/4.0/>).

Reuse

This article is distributed under the terms of the Creative Commons Attribution-NonCommercial-NoDerivs (CC BY-NC-ND) licence. This licence only allows you to download this work and share it with others as long as you credit the authors, but you can't change the article in any way or use it commercially. More information and the full terms of the licence here: <https://creativecommons.org/licenses/>

Takedown

If you consider content in White Rose Research Online to be in breach of UK law, please notify us by emailing eprints@whiterose.ac.uk including the URL of the record and the reason for the withdrawal request.



eprints@whiterose.ac.uk
<https://eprints.whiterose.ac.uk/>

1 **Assessment of semi-mechanistic bubble departure diameter modelling for the** 2 **CFD simulation of boiling flows**

3
4 **Marco Colombo*¹, Ronak Thakrar², Michael Fairweather¹ and Simon P. Walker²**

5
6 ¹ School of Chemical and Process Engineering
7 University of Leeds, Leeds, LS2 9JT, United Kingdom

8
9 ² Department of Mechanical Engineering, Imperial College London, Exhibition Road, London,
10 SW7 2AZ, United Kingdom

11
12 * Corresponding Author: M.Colombo@leeds.ac.uk; +44 (0) 113 343 2351

13
14 © 2019. This manuscript version is made available under the CC-BY-NC-ND 4.0 license

15 <http://creativecommons.org/licenses/by-nc-nd/4.0/>

16 Published paper <https://doi.org/10.1016/j.nucengdes.2019.01.014>

17 18 **ABSTRACT**

19
20 Eulerian-Eulerian two-fluid computational fluid dynamic (CFD) models are increasingly applied
21 to predict multiphase and boiling flows in nuclear reactor thermal hydraulics. In these models,
22 nucleate boiling is usually accounted for by partitioning the heat flux between the different
23 mechanisms of heat transfer involved. Although structured in a mechanistic fashion, heat flux
24 partitioning models are still forced to rely on mainly empirical closure relations. Between the
25 numerous closures required, the bubble departure diameter in particular has a significant
26 influence on the predicted interfacial area concentration and void distribution within the flow.
27 There is now abundant evidence in the literature of the limited accuracy and reliability of the
28 empirically-based correlations that are normally applied in CFD models. In view of this, in this
29 work more mechanistic formulations of bubble departure have been introduced into the STAR-
30 CCM+ code. The models are based on a balance of the hydrodynamic forces that act on a bubble
31 at the nucleation site. Their performance, and compatibility with existing implementations in a
32 CFD framework, are assessed against two different data sets for vertically upward subcooled
33 boiling flows. In general, a significant number of modelling choices is required by these
34 mechanistic models and some recommendations are made. The models are extended to include a
35 more physically-consistent coupled calculation of the frequency of bubble departure. In general,
36 predictions of the wall temperature reach a satisfactory accuracy, even if numerous numerical
37 and modelling uncertainties are still present. In view of this, several areas for future work and

38 modelling improvement are identified, such as the proper modelling of the local subcooling
39 acting on the bubble cap.

40

41 **KEYWORDS**

42 Nucleate boiling, computational fluid dynamics, bubble departure diameter, semi-mechanistic
43 model

44

45 **1. INTRODUCTION**

46

47 Boiling is a very efficient heat transfer mechanism and the convenience of transferring large
48 amounts of heat with minimum temperature differences is exploited in numerous industrial and
49 engineering sectors. Practically all water-cooled nuclear reactors experience some degree of
50 boiling, during the normal operation of the plant or in design-basis and beyond design-basis
51 postulated accidents. However, the physics of boiling and the mechanisms triggering a boiling
52 crisis (often referred to as the departure from nucleate boiling (DNB) or dryout), still lack robust
53 and reliable modelling and comprehensive understanding (Bestion, 2012; Yadigaroglu, 2014). In
54 recent years, computational fluid dynamics (CFD) has proved of value in the prediction of
55 multiphase flows and multiphase nuclear reactor thermal hydraulics. CFD can capture physical
56 processes across large ranges of length scales and with finer spatial and temporal resolution than
57 conventional ‘system code based’ thermal hydraulic approaches. Therefore, CFD methods are
58 appealing for the prediction of boiling and the critical heat flux, which is the maximum amount
59 of heat that is safely transferrable before triggering the boiling crisis.

60

61 In recent years, many attempts have been made to incorporate wall boiling models into CFD
62 codes and specifically in the two-fluid models that are most often used to tackle component-scale
63 engineering problems. Most commercial CFD platforms include inside their two-fluid averaged
64 models some boiling capability that is typically based on the Rensselaer Polytechnic Institute
65 (RPI) heat flux partitioning model introduced by Kurul and Podowski (1990). In this model, the
66 heat flux from the wall is partitioned between the mechanisms that are presumed to be
67 responsible for the heat transfer process; single-phase convection, quenching and evaporation.
68 Although the RPI model and all its more recent modifications are structured in a mechanistic
69 fashion, they rely on numerous mostly empirical or semi-empirical closure relations (Krepper
70 and Rzehak, 2011; Koncar and Matkovic, 2012; Thakrar et al., 2017). The evaporative heat

71 transfer component, in particular, requires closures for the active nucleation site density, the
72 bubble departure diameter and the bubble departure frequency to calculate the rate of phase
73 change at the wall. In most CFD studies to date, these have been predicted with different
74 empirical correlations. The numerous correlations available have been reviewed in Thakrar et al.
75 (2014) and Cheung et al. (2014) and were found in both studies to usually have limited accuracy
76 and generality. The wider applicability of the RPI model is thus limited and calibration has been
77 often required to accurately predict boiling flow data sets under investigation (Yeoh and Tu,
78 2006; Krepper et al., 2013; Colombo and Fairweather, 2016a). It is therefore expected that the
79 predictive capability of the RPI model can be improved by gradually replacing the current mostly
80 empirical closures in favour of more mechanistic sub-modelling.

81
82 This paper investigates the semi-mechanistic modelling of the bubble departure diameter closure.
83 In the RPI model, the value of the departure diameter is required to calculate the evaporative heat
84 flux and the portion of the wall surface where boiling is the dominant heat transfer mechanism.
85 In addition, the bubble departure diameter determines the wall nucleation source in population
86 balance models. These are normally coupled to the two-fluid framework and track the evolution
87 of the bubble diameter distribution in the flow (Yao and Morel, 2004; Yun et al., 2012; Colombo
88 and Fairweather, 2016a). Therefore, the accuracy of this particular closure has a large impact
89 upon predicted mean flow quantities, including the void fraction distribution and the temperature
90 field in the liquid.

91
92 In recent decades, more mechanistic approaches for predicting the departure diameter under pool
93 and forced convective boiling conditions have been proposed. These originate from the model of
94 Klausner et al. (1993). In this model, bubble growth is computed from an approach based on the
95 diffusion of heat into the bubble from the surrounding liquid. Detachment of the bubble from the
96 nucleation cavity is evaluated from a balance of the hydrodynamic forces that act on the bubble.
97 The model, validated against measurements in refrigerant R113 under saturated boiling
98 conditions, was later extended to both pool and flow boiling (Zeng et al., 1993a; Zeng et al.,
99 1993b). Over the years, subsequent modelling efforts have largely attempted to calibrate
100 Klausner et al.'s model to extend its predictive capability to cover a wider range of experimental
101 conditions (Situ et al., 2005; Wu et al., 2008). Sugrue and Buongiorno (2016) calibrated

102 Klausner et al.'s model against several low-pressure data sets by making adjustments to the
103 contact diameter model. Other authors have included additional heat transfer mechanisms to the
104 existing models, mainly based on the growth of a bubble in an infinite uniformly superheated
105 liquid (Forster and Zuber, 1954; Plesset and Zwick, 1954). Yun et al. (2012) introduced the effect
106 of local condensation into the bubble growth rate model and suggested modifications to both the
107 lift force and the surface tension models. Colombo and Fairweather (2015) extended Yun et al.'s
108 (2012) model by including the contribution of microlayer evaporation beneath the bubble based
109 on the approach of Cooper and Lloyd (1969). The same microlayer model, with a modified
110 growth equation to account for local condensation on the bubble cap, was recently applied by
111 Mazzocco et al. (2018). Whilst these models continue to incorporate a significant empirical
112 component, it is hoped nevertheless that the more local considerations involved will extrapolate
113 more effectively toward high-pressure pressurized water reactor (PWR) conditions, where
114 measurements of diameter are scarce for obvious reasons.

115
116 Overall, these models have rarely been implemented inside CFD codes (Yun et al., 2012; Yeoh et
117 al., 2014; Gilman and Baglietto, 2017). Even less frequent have been analyses focused on the
118 force-balance model itself, particularly in relation to the local near-wall flow conditions that are
119 required as input, normally at a length scale smaller than the first near-wall finite-volume cell, in
120 particular at high pressure. Recently, Thakrar and Walker (2016) undertook an evaluation of the
121 force-balance model of Sugrue and Buongiorno (2016) in the STAR-CCM+ commercial code
122 (CD-adapco, 2016). Authors were able to predict reasonably well the popular high pressure
123 subcooled boiling test case of Bartolomei and Chanturiya (1967), most computations of this test
124 case having used a bubble departure diameter obtained from empirical correlations. Amongst
125 numerous options, correlations from Tolubinsky and Kostanchuk (1970) and
126 Kocamustafaogullari (1983) are frequently used. Being derived from mean parametric data, these
127 are not, however, equipped to reflect the dependency on the local flow conditions that are
128 normally available in a CFD calculation (Thakrar and Walker, 2016).

129
130 In this work, three force balance models, from Klausner et al. (1993), Yun et al. (2012) and
131 Sugrue and Buongiorno (2016), are implemented in the STAR-CCM+ code (CD-adapco, 2016).
132 The performance of the CFD model is assessed blindly against the experiments of Bartolomei

133 and Chanturiya (1967) and Garnier et al. (2001) (referred to more commonly as the DEBORA
 134 benchmark) for subcooled boiling flows of water and refrigerant in vertical pipes. Although not
 135 entirely similar, these experiments were selected to replicate as closely as possible elevated
 136 pressure operating conditions in PWRs. Results are also compared with the most frequently used
 137 empirical correlations. Impacts on the results of different modelling choices are examined and
 138 results of the force balance analyzed and possible improvements in the modelling of some forces
 139 are suggested. Bubble departure frequency is also directly evaluated from the force balance
 140 model, improving the internal physical consistency of the model. Finally, some sensitivity
 141 studies are made on the modelling of condensation on the bubble cap.

142
 143 **2. EXPERIMENTAL DATA**
 144

145 Two experiments have been predicted in this work, from the database of Bartolomei and
 146 Chanturiya (1967) and the DEBORA experiment (Garnier et al., 2001), with the specific
 147 conditions considered reported in Table 1.

148
 149 Table 1. Experimental conditions of the two test cases.
 150

Experiment	p [MPa]	G [kg m ⁻² s ⁻¹]	q [kWm ⁻²]	T _{in} [°C]	D [m]	Fluid
Bartolomei and Chanturiya	4.5	900	570	197.4	0.0154	Water
DEBORA	2.62	1985	73.9	70.5	0.0192	R12

151
 152 Bartolomei and Chanturiya (1967) investigated the subcooled boiling of water flowing upward in
 153 a vertical pipe of inner diameter $D = 0.0154$ m and length $L = 2$ m. Area-averaged void fractions
 154 were measured using a gamma-ray attenuation technique driven by a Thulium-170 source at
 155 different axial locations and at pressures up to 15 MPa, mass fluxes up to 2000 kg m⁻² s⁻¹ and
 156 heat fluxes up to 2.2 MW m⁻². In addition, wall temperature, axial liquid temperature and area-
 157 averaged liquid temperature measurements were also provided for the 4.5 MPa case, and,
 158 therefore, this specific experiment is simulated here.

159
 160 The DEBORA (Garnier et al., 2001) flow loop consisted of a 19.2 mm inner diameter vertical
 161 pipe, heated for a length of 3.5 m and operated with Freon-12 (R-12). It is both difficult and
 162 expensive to measure the flow boiling behaviour of water at high pressure. Employing R-12 as
 163 the working fluid partially replicates the flow characteristics of a prototypical high pressure flow

164 of water under much milder conditions. In the range of pressures investigated in the DEBORA
165 experiment (1.46 – 3.01 MPa), the values of the relevant dimensionless groups for R-12, such as
166 the Reynolds and Weber numbers, and the density ratio, are comparable to those found in PWRs.
167 Void fraction and vapour velocity profiles at the end of the test section were measured with an
168 optical probe technique, from which radial profiles of the interfacial area concentration and the
169 Sauter mean diameter (SMD) were determined. Thermocouples were used to measure the liquid
170 temperature radial profile and the wall temperature at selected axial locations. Details of the
171 specific experiment investigated here, characterized by a pressure of 2.62 MPa, are given in
172 Table I.

173

174 Measurements of the bubble departure diameter are not provided by either of the two
175 experiments. Such measurements, particularly under forced convective conditions, are
176 understandably quite scarce at elevated pressure. Similarly, data for mean flow quantities under
177 prototypic reactor operating conditions (~ 15 MPa) is equally scarce. The two databases selected
178 are amongst the most frequently employed for validating CFD boiling predictive capability, and
179 represent an appropriate compromise between data availability and proximity to true nuclear
180 reactor operating conditions.

181

182 **3. MATHEMATICAL MODEL**

183

184 In a two-fluid Eulerian-Eulerian model, each phase is described by a set of time averaged
185 conservation equations, and the continuity, momentum and energy equations are solved for each
186 phase. These are discussed in many previous publications, such as Ishii and Hibiki (2006), and
187 are not presented here. Instead, the description is focused on the wall boiling and the bubble
188 departure diameter models, these being the main subject of the work. Implementation of all the
189 other models follows a standard approach and a full description of the models as well as the
190 values of the many modelling parameters employed can be found in CD-adapco (2016). The drag
191 model of Tomiyama et al. (1998) is used with the model of Burns et al. (2004) for the turbulent
192 dispersion. Lift and wall lubrication forces are not included. Although both might affect boiling
193 modelling, their role and magnitude in boiling flows is not well-understood and unlikely to be
194 predicted with accuracy by models designed for adiabatic bubbly flows. A standard high-
195 Reynolds multiphase version of the k - ϵ turbulence model (Jones and Launder, 1972) solves for

196 the turbulence in the liquid phase, whereas in the vapour phase the turbulence is directly related
 197 to that in the liquid using a turbulence response model (in this case with the turbulence in both
 198 phases being equal).

199

200 Bubbles, after their departure from the heated wall, experience evaporation and condensation in
 201 the bulk of the flow, and break-up and coalescence events that alter the bubble diameter
 202 distribution and affect the interphase mass, momentum and energy exchanges. The bubble
 203 diameter distribution is predicted with the S_γ model (Lo and Zhang, 2009). Moments of the
 204 bubble diameter distribution, which is assumed to obey to a pre-defined log-normal shape, are
 205 calculated and used to define the SMD in the flow:

206

$$S_\gamma = nM_\gamma = n \int_0^\infty d_B^\gamma P(d_B) d(d_B) \quad (1)$$

207

208 The one-equation version of the model is considered (CD-adapco, 2016) and the transport
 209 equation for the second moment of the bubble distribution is solved to find the SMD:

210

$$\frac{\partial S_\gamma}{\partial t} + \nabla \cdot (S_\gamma \mathbf{U}_v) = S_{br}^\gamma + S_{cl}^\gamma \quad (2)$$

$$d_{SM} = d_{32} = \frac{S_3}{S_2} = \frac{6\alpha}{a_i} \quad (3)$$

211

212 Breakup and coalescence models are taken from Yao and Morel (2004) and adapted following
 213 the work of Colombo and Fairweather (2016b), where they were successfully validated against
 214 air-water bubbly flows. Here, a value of 1.24 is used for the critical Weber number We_{cr} . Finally,
 215 condensation and evaporation in the bulk of the fluid are evaluated from the Ranz and Marshall
 216 (1952) correlation.

217

218 ***3.1 Wall Heat Flux Partitioning Model***

219

220 When nucleate boiling takes place at the wall, wall superheat and the related heat transfer
 221 coefficient, and the temperature in the wall-adjacent finite-volume cell, are obtained from the
 222 solution of the wall heat flux partitioning model. Following the RPI approach, the total heat flux
 223 is partitioned between the mechanisms responsible for heat removal:

224

$$q_w = (q_l + q_q + q_{ev})(1 - K_{dry}) + K_{dry}q_v \quad (4)$$

225
226
227
228
229
230
231
232
233
234
235
236
237
238

Latent heat is removed by evaporation (q_{ev}) and supports the growth of vapour bubbles at the active nucleation sites. Detachment of these bubbles promotes additional mixing by drawing in cooler liquid in the space previously occupied by the bubble, causing rewetting of the heating surface, and this additional contribution to the total heat transfer (q_q) is often referred to as quenching. In regions of the wall not affected by boiling, sensible heat is transferred to the liquid-phase by ordinary single-phase convection (q_l). Finally, if the amount of vapour generated at the wall is high enough so as to begin to obstruct surface rewetting, a portion of the wall heat is transferred by convection to the vapour phase (q_v). In this case, the fraction of the wall surface in contact with the vapour phase is represented by K_{dry} , which becomes larger than zero when the void fraction is higher than a critical value, assumed equal to 0.9. The heat flux for the single-phase convective contribution is evaluated using standard wall treatments and using the temperature in the near-wall cell T_l , as illustrated below:

$$q_l = (1 - A_b)h_l(T_w - T_l) = (1 - A_b)\frac{\rho_l C_{p,l} u_{\tau,l}}{T_l^+} (T_w - T_l) \quad (5)$$

239
240
241
242
243
244
245
246

The boiling area fraction A_b is the fraction of the wall affected by the evaporation process and T_l^+ is the dimensionless temperature in the near-wall cell. The convective heat flux to the vapour phase is calculated in a similar way. The quenching heat flux is expressed as the product of a quenching heat transfer coefficient, modelled as a transient conduction into a semi-infinite medium (Del Valle and Kenning, 1985), and the temperature difference between the wall and the liquid:

$$q_q = A_b h_q (T_w - T_l) = 2A_b f \sqrt{\frac{\rho_l C_{p,l} \lambda_l t_w}{\pi}} (T_w - T_l) \quad (6)$$

247
248
249
250
251

In the previous equation, the waiting time t_w is equal to 80 % of the total ebullition cycle of a bubble, known from the inverse of the bubble departure frequency f , and, to avoid any dependency on the computational grid, the liquid temperature is evaluated at a constant wall y^+ of 250. The evaporative heat flux is known from the mass flux of bubbles generated at the wall

252 and the latent heat of vaporization i_{lv} . Assuming the bubbles are spherical, this mass flux is easily
253 computed from the number of nucleation sites active per unit area N_A , the bubble departure
254 diameter d_{dep} and the bubble departure frequency f :

$$q_{ev} = N_A f \left(\frac{\pi d_{dep}^3}{6} \right) \rho_v i_{lv} \quad (7)$$

256
257 The nucleation site density and bubble departure diameter are also used to derive the fraction of
258 the wall exposed to the boiling process:

$$A_b = 2.0 \frac{\pi d_{dep}^2}{4} N_A \quad (8)$$

260
261 It is clear that predictions of the heat flux partitioning model are strongly related to the closure
262 models for the active nucleation site density, the bubble departure diameter and the bubble
263 departure frequency. Normally, these are predicted using empirical closures that, being mostly
264 derived from bulk parameters, show limited accuracy and applicability, and solutions that are
265 frequently grid-dependent. Correlations for the active nucleation site density in particular are
266 associated with significant uncertainty related to the specific conditions of the surface. This is not
267 addressed in the present paper and the site density is predicted using the correlation of Hibiki and
268 Ishii (2006), which has been shown to give a $\sim 50\%$ error for high pressure water flows.

269
270 The bubble departure diameter is calculated from a force balance approach. More specifically,
271 bubble growth is predicted from an energy balance that accounts for the different mechanisms of
272 heat transfer between the bubble and the wall, and the surrounding liquid. The departure
273 condition is evaluated from balances of the forces acting on the bubble in directions parallel (x)
274 and perpendicular (y) to the heated wall. Depending on the balance that is violated first,
275 therefore, the departure diameter used by the heat flux partitioning model is the diameter at
276 which the bubble departs (parallel) and begins to slide away from the nucleation site and along
277 the wall, or lifts-off (perpendicular), moving away from the wall and towards the bulk of the
278 flow. The much greater heat fluxes required to drive boiling at elevated pressures cause bubbles
279 to lift-off very quickly (Thakrar and Walker, 2016). It is thus reasonable to assume that bubbles
280 lift-off immediately following departure at the conditions investigated here.

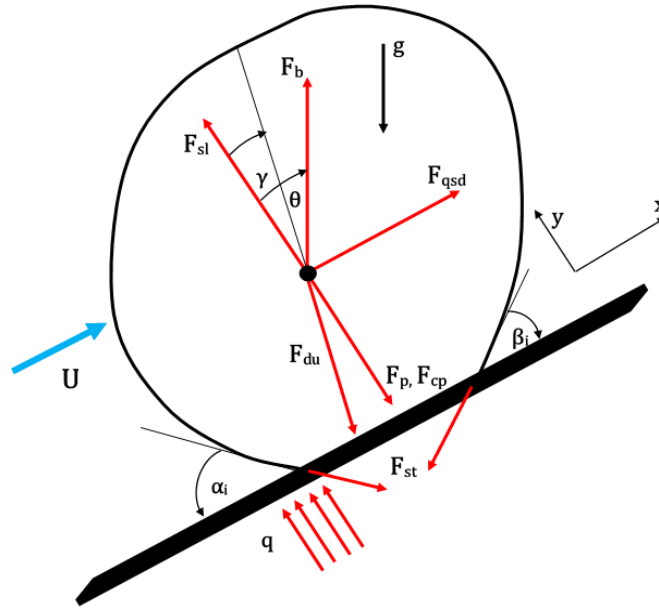


Figure 1. Forces acting on a bubble at the nucleation site.

281
 282
 283
 284 The three force balance models from Klausner et al. (1993), Yun et al. (2012) and Sugrue and
 285 Buongiorno (2016) were applied. As discussed previously, the latter two are extensions of the
 286 former, which was developed and validated against flow boiling of R113 in a square duct at
 287 atmospheric pressure. Specifically, instead of the constant contact diameter d_w employed by
 288 Klausner et al. (1993), both introduced a variable value calculated as a fraction of the bubble
 289 diameter. Sugrue and Buongiorno (2016) employed $d_w / d_B = 0.025$, while the value 0.067 was
 290 adopted by Yun et al. (2012). The force balance considers several forces: the surface tension
 291 force $F_{stx/sty}$ that keeps the bubble attached to the wall; the buoyancy force F_b that promotes the
 292 departure of the lower density bubble; the quasi-steady drag force F_{qs} and the shear lift force F_{sl} ,
 293 quantifying the tendency of the fluid flow to strip the bubble from the nucleation site; the
 294 unsteady drag force due to asymmetrical bubble growth $F_{dux/duy}$, representing the opposition to
 295 bubble growth exercised by the fluid that surrounds the bubble; and the pressure forces over the
 296 bubble surface, split between the hydrodynamic force F_p and the contact pressure force F_{cp} (see
 297 Figure 1). No additional modifications to these forces have been introduced, although their
 298 applicability to the conditions investigated is still unclear and, inevitably, the modelling still
 299 relies on a number of empirical parameters. Between these parameters, the only small difference
 300 is the value of the shear lift coefficient C_l that Yun et al. (2012) fix at 0.118, higher than both
 301 Klausner et al. (1993) and Sugrue and Buongiorno (2016). For both the Klausner et al. (1993)
 302 and Sugrue and Buongiorno (2016) models, the bubble growth equation from Forster and Zuber

303 (1954) with a value of $b = 1.56$ is used, this being the asymptotic solution of the Mikic and
304 Rohsenow (1969) model that was originally adopted by Klausner et al. (1993). A similar
305 modification to the original Klausner et al. (1993) model was introduced in the subsequent paper
306 from Zeng et al. (1993a). Instead, Yun et al. (2012) added to the Forster and Zuber (1954) growth
307 equation the contribution of the locally subcooled flow, and the condensation heat transfer
308 coefficient was evaluated using the Ranz and Marshall (1952) model. In the results section,
309 predictions of the three models are also compared with the widely applied correlations of
310 Tolubinsky and Kostanchuk (1970) and Kocamustafaogullari (1983). Details of all the models
311 adopted, the force balance and the growth equation are summarized in Table 2.

312

313 Initially, the bubble departure frequency was calculated from the correlation of Cole (1960).
314 However, the force balance model assumes a growth rate equation, and the growth time that is
315 derived from this may contradict the value of the departure frequency predicted using Cole's
316 (1960) correlation. In this work, the departure frequency is obtained directly from the growth rate
317 equation, with the growth time assumed to make up 20% of the total ebullition period (Kurul and
318 Podowski, 1990). The results are then compared against Cole's (1960) correlation. In order to
319 examine the impact of condensation effects, implementation of the Yun et al. (2012) force
320 balance model is undertaken excluding in the first instance any contribution of condensation in
321 the growth rate equation. It is worth remarking that the latter authors do not describe how the
322 liquid temperature used in their growth rate equation is determined. Whilst this is expected to be
323 the local temperature, indirect evidence suggests that the wall cell temperature was in fact
324 employed. In the interests of remaining consistent with the original form of the model, similar
325 assumptions are employed herein.

326

327

328

329

330

331

332

333

334
335

Table 2. Summary of the models for bubble departure diameter and bubble departure frequency.

Model	Form
Force balance	$\sum F_x = F_{stx} + F_{qsd} + F_b \sin \theta + F_{dux} = 0$ $\sum F_y = F_{sty} + F_{sl} + F_b \cos \theta + F_{duy} + F_p + F_{cp} = 0$ $F_{stx} = -1.25d_w\sigma \frac{\pi(\alpha_i - \beta_i)}{\pi^2 - (\alpha_i - \beta_i)^2} (\sin \alpha_i - \sin \beta_i)$ $F_{sty} = -d_w\sigma \frac{\pi}{(\alpha_i - \beta_i)} (\cos \beta_i - \cos \alpha_i)$ $F_{qsd} = 6\pi\rho_l\nu UR \left\{ \frac{2}{3} + \left[\left(\frac{12}{Re} \right)^{0.65} + 0.862 \right]^{-1.54} \right\}$ $F_{du} = -\rho_l\pi R^2 \left(\frac{3}{2}\dot{R}^2 - R\ddot{R}^2 \right)$ $F_b = \frac{4}{3}\pi R^3(\rho_l - \rho_v)g$ $F_{sl} = \frac{1}{2}\pi\rho_l U^2 R^2 \{ 3.877G_s^{0.5} [Re^{-2} + (C_l G_s^{0.5})^4]^{0.25} \}$ $F_p = \frac{9}{8}\rho_l U^2 \frac{\pi d_w^2}{4}$ $F_{cp} = \frac{\sigma \pi d_w^2}{R \cdot 4}$ $R(t) = \frac{2b}{\sqrt{\pi}} J a \sqrt{at}; b = 1.56$
Klausner et al. (1993)	$d_w = 0.09 \text{ mm} \quad C_l = 0.014$
Sugrue and Buongiorno (2016)	$d_w/d_b = 0.025 \quad C_l = 0.014$
Yun et al. (2012)	$d_w/d_b = 0.067 \quad C_l = 0.118$ $R(t) = \frac{2b}{\sqrt{\pi}} J a \sqrt{at} - \frac{bq_c}{Si_{lv}\rho_v} t; b = 1.56; S = 2$
Tolubinsky and Kostanchuk (1970)	$d_{dep} = d_0 \exp[-(T_{sat} - T_l)/\Delta T_0] \quad d_0 = 0.006 \text{ mm} \quad \Delta T_0 = 45 \text{ K}$
Kocamustafaogullari (1983)	$d_{dep} = d_0 \theta \left(\frac{\sigma}{g\Delta\rho} \right)^{0.5} \left(\frac{\Delta\rho}{\rho_v} \right)^{0.9} \quad d_0 = 0.0015126 \text{ mm} \quad \theta = 0.722 \text{ rad}$
Cole (1960)	$f = \sqrt{\frac{4}{3} \frac{g(\rho_l - \rho_v)}{d_{dep}\rho_l}}$
Waiting time	$t_w = 0.8/f$

336
337

3.2 Numerical Implementation

338

339

340

341

342

The overall model was solved using the steady-state solver of the STAR-CCM+ CFD code (CD-adapco, 2016). A two-dimensional axisymmetric geometry was employed and, at the inlet, a fully-developed single-phase liquid velocity, turbulence and temperature were imposed, together

343 with an imposed pressure at the outlet and the no-slip condition, and an imposed heat flux, at the
344 wall. Specifically, inlet profiles were obtained, in the same geometrical domain, by performing
345 single-phase calculations until fully-developed conditions were achieved at the same mass flow
346 rate, with the resulting steady conditions used as initial conditions for subsequent multi-phase
347 calculations. Constant thermophysical properties were used for both phases. More specifically,
348 liquid properties were calculated at the average temperature between the inlet and saturation, and
349 matched carefully against the experimental inlet mass flux. Vapour properties were calculated at
350 saturation. A mesh sensitivity study demonstrated that grid-independent solutions (with a total
351 number of grid elements equal to 20×375 for the Bartolomei and Chanturiya (1967), and $20 \times$
352 750 for the DEBORA, test cases) were achieved with an equidistant structured mesh that ensured
353 the minimum wall y^+ value was greater than 30, the latter being sufficiently high to justify the
354 high-Reynolds number wall treatment selected.

355 356 **4. RESULTS AND DISCUSSION**

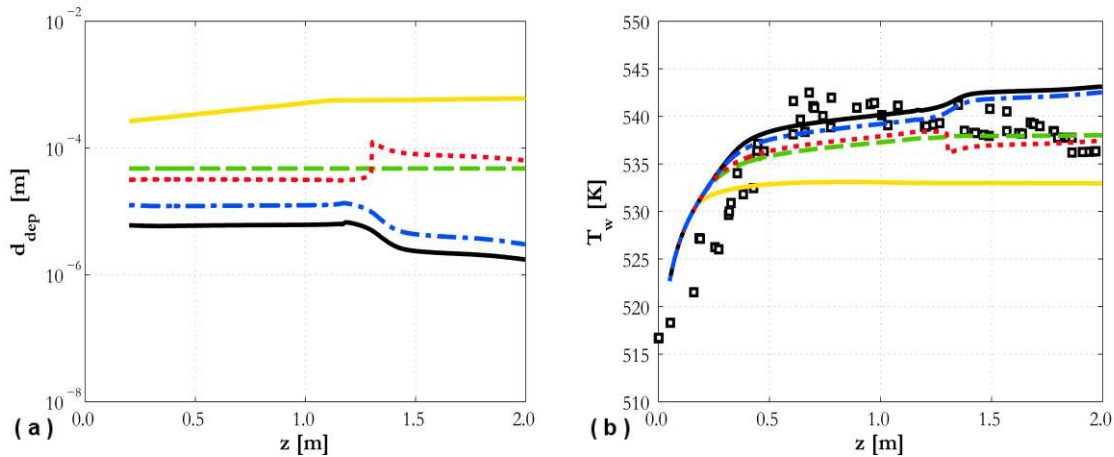
357
358 The first set of results is shown in Figures 2 and 3 for the two experiments. Predictions from the
359 three force balance models (Klausner et al., 1993; Yun et al., 2012; Sugrue and Buongiorno,
360 2016), neglecting subcooling in the Yun et al. case, coupled with the Cole (1960) correlation for
361 bubble departure frequency, are compared against wall temperature data, and predictions of the
362 Tolubinsky and Kostanchuk (1970) and Kocamustafaogullari (1983) correlations. Bubble
363 departure diameter predictions are generally spread over a few orders of magnitude, even if this
364 translates into differences in the wall temperature that are limited to a 10 K range for the data in
365 Figure 2(b) and 5 K for that in Figure 3(b).

366
367 Some issues with the Klausner et al. (1993) model are immediately apparent from Figure 2. At a
368 certain distance from the inlet, a well-defined step is found in both the bubble departure diameter
369 and the wall temperature. Further downstream, a solution for the lift-off diameter could not be
370 found and the model is forced to revert back to the bubble departure solution, if available, or the
371 default value given by the Kocamustafaogullari (1983) correlation. In contrast, upstream a
372 solution for the lift-off diameter was successfully computed, causing the abrupt step in the value
373 of the departure diameter. This inconsistency is related to the constant contact diameter d_w used
374 in the Klausner et al. (1993) model, which, for the specific conditions studied, is sometimes even

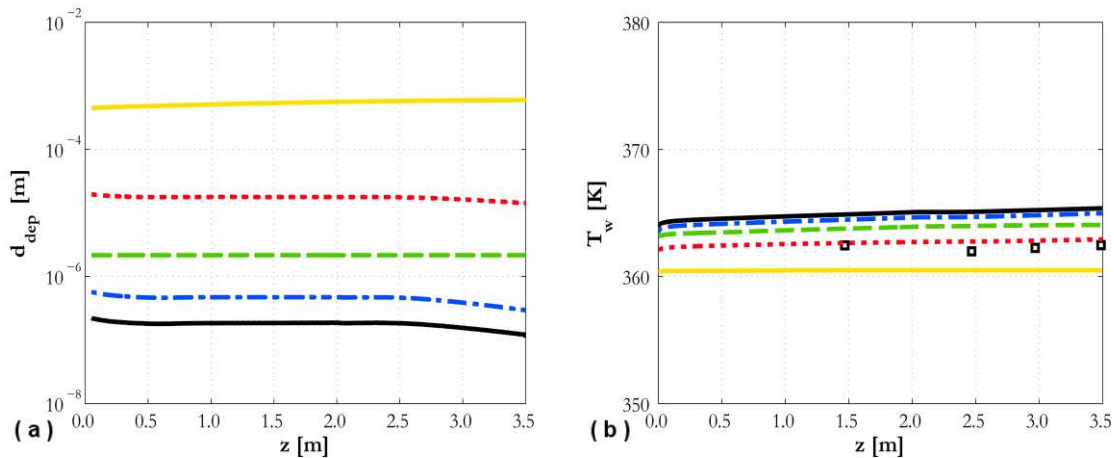
375 higher than the bubble diameter and, therefore, prevents the code reaching an acceptable
376 (positive) solution. Even if the same inconsistency is not found in Figure 3, a value of d_w that
377 depends on the bubble diameter, such as that adopted by Sugrue and Buongiorno (2016) and Yun
378 et al. (2012), is clearly preferable. Such models consistently report positive solutions for both
379 force balances. The force balance parallel to the wall is broken first, suggesting that the bubbles
380 may slide first before lifting off. Reasonable agreement with the Bartolomei and Chanturiya
381 (1967) experiment is found, except in the final section of the pipe, where a sudden increase in
382 wall temperature is predicted by both the Sugrue and Buongiorno (2016) and Yun et al. (2012)
383 models. In the DEBORA experiment, the wall temperature is over predicted, although not
384 excessively.

385
386 The Kocamustafaogullari (1983) correlation predicts values in the neighborhood of the force
387 balance results. A constant value is predicted because the correlation is only a function of
388 pressure, once the fluid properties are assumed constant with temperature. In contrast, the
389 Tolubinsky and Kostanchuk (1970) correlation returns very high values of the bubble departure
390 diameter and, consequently, under predicts the wall temperature. This was already observed by
391 Thakrar and Walker (2016) for the Bartolomei and Chanturiya (1967) experiment, and
392 confirmation is found here for the DEBORA experiment. For this reason, the Tolubinsky and
393 Kostanchuk (1970) correlation is not used in the following comparisons. In a similar way, and in
394 agreement with the preceding discussion, only the Sugrue and Buongiorno (2016) and Yun et al.
395 (2012) models are considered below.

396
397
398
399



400
 401 Figure 2. Predicted bubble departure diameter (a) and wall temperature (b) for Bartolomei and
 402 Chanturiya (1967) experiment: (\square) data; (—) Tolubinsky and Kostanchuk (1970); (---)
 403 Kocamustafaogullari (1983); (···) Klausner et al. (1993); (—) Sugrue and Buongiorno (2016);
 404 (— · —) Yun et al. (2012) without subcooling. Bubble departure frequency from Cole (1960).
 405

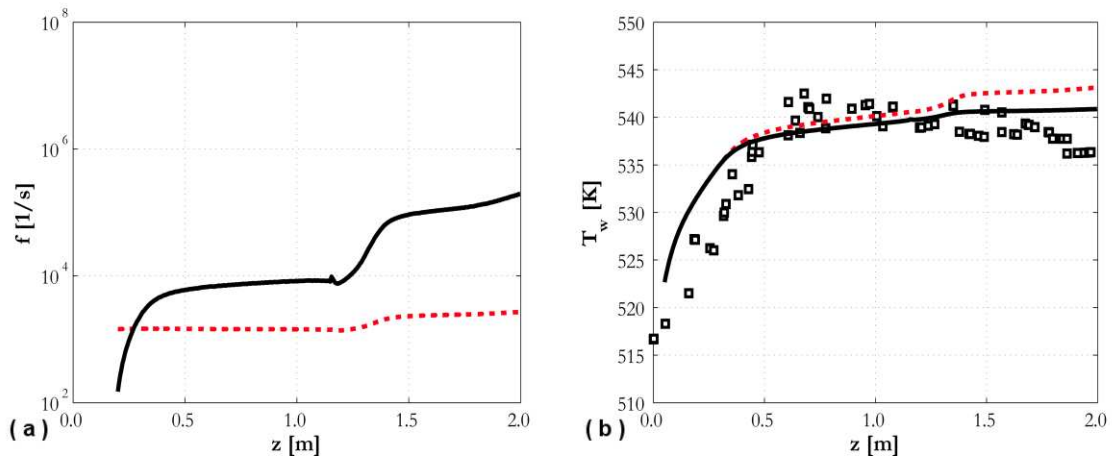


406
 407 Figure 3. Predicted bubble departure diameter (a) and wall temperature (b) for DEBORA
 408 experiment (Garnier et al., 2001): (\square) data; (—) Tolubinsky and Kostanchuk (1970); (---)
 409 Kocamustafaogullari (1983); (···) Klausner et al. (1993); (—) Sugrue and Buongiorno (2016);
 410 (— · —) Yun et al. (2012) neglecting subcooling. Bubble departure frequency is calculated from
 411 Cole (1960).
 412

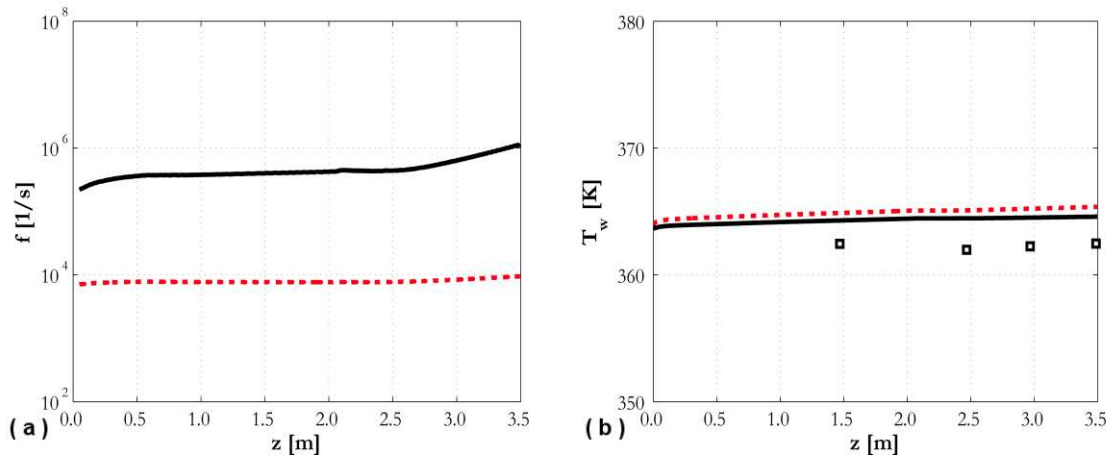
413 In Figures 2 and 3, the Cole (1960) model was used to predict the bubble departure frequency. In
 414 Figures 4 and 5, the bubble growth time from the departure routine was used to evaluate the
 415 frequency of bubble departure and this is compared against Cole (1960), using the Sugrue and
 416 Buongiorno (2016) bubble departure model. Clearly, using a frequency decoupled from the
 417 bubble departure diameter calculation can generate physical inconsistencies in the solution that
 418 can overcome the benefits of the more mechanistic bubble departure model. More specifically,
 419 near the end of the pipe, the departure diameter decreases (Figure 2(a)) but the frequency from

420 Cole (1960) remains almost constant (Figure 4(a)). This, from Eq. (7), reduces the evaporative
 421 heat flux, causing the increase in wall temperature observed in Figures 2(b) and 4(b). Using the
 422 calculated departure time, a decrease in departure diameter corresponds to a faster growth time
 423 and an increase in frequency. Therefore, the evaporative heat flux does not decrease and a flatter
 424 temperature profile is found that is more in agreement with the experiments (Figure 4(b)).
 425 Similar findings are found for the DEBORA experiment, as shown in Figure 5. A reduction in
 426 the departure diameter is reflected in a higher departure frequency and a wall temperature
 427 slightly more in agreement with experiments. Overall, the coupled departure diameter and
 428 frequency calculation improves the internal consistency of the model and the predicted frequency
 429 may differ from Cole (1960) by up to two orders of magnitude.

430



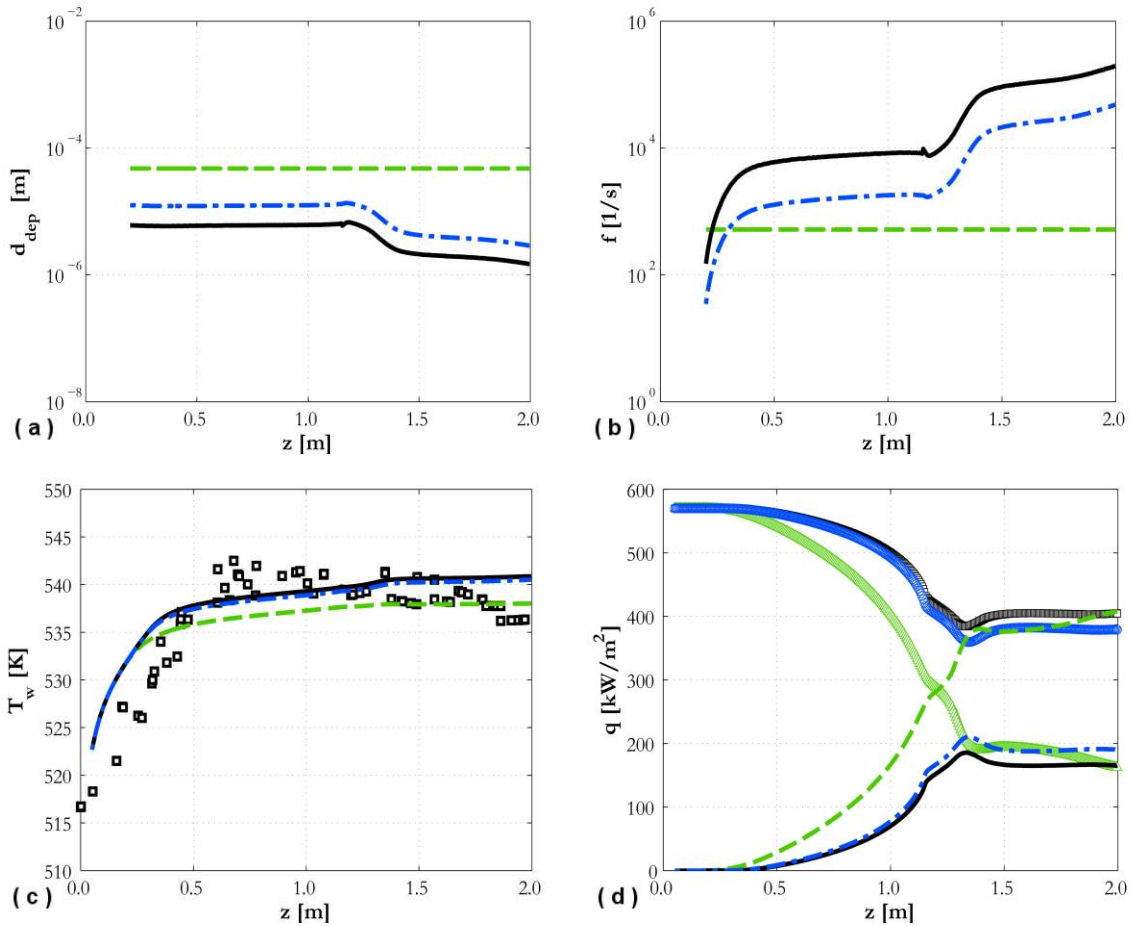
431
 432 Figure 4. Predicted bubble departure frequency (a) and wall temperature (b) for Bartolomei and
 433 Chanturiya (1967) experiment using Sugrue and Buongiorno (2016) model: (\square) data; (\cdots) Cole
 434 (1960) model; (—) frequency derived from departure time.
 435



436
 437 Figure 5. Predicted bubble departure frequency (a) and wall temperature (b) for DEBORA
 438 experiment (Garnier et al., 2001) using Sugrue and Buongiorno (2016) model: (\square) data; (\cdots) Cole
 439 (1960) model; (—) frequency derived from departure time.
 440

441 Overall comparisons of departure diameter, frequency, wall temperature and heat fluxes are
 442 reported in Figures 6 and 7. The Sugrue and Buongiorno (2016) and Yun et al. (2012) models,
 443 the latter still neglecting the subcooling contribution, return rather similar predictions, with the
 444 latter predicting a higher bubble departure diameter and lower frequency, and slightly lower wall
 445 temperature and higher evaporative heat flux. Acceptable agreement is found with wall
 446 temperature measurements, even if the observed reduction in wall temperature at the end of the
 447 pipe in the Bartolomei and Chanturiya (1967) experiment is not reproduced. This is associated
 448 indirectly with local flow acceleration in the high void fraction region, and the resulting
 449 reduction in predicted diameter under these conditions. Because the partitioning model employed
 450 does not consider the effects of coalescence, the trends illustrated are indicative of isolated
 451 boiling conditions, and do not reflect the true departure diameter in this region. In the DEBORA
 452 experiment, the wall temperature is over predicted, although not excessively. No sharp decrease
 453 in the force balance predicted departure diameter is observed downstream in the DEBORA
 454 experiment, presumably due to the much lower void fraction prediction in this experiment.

455



456

457

458

459

460

461

462

463

464

465

466

467

468

469

470

471

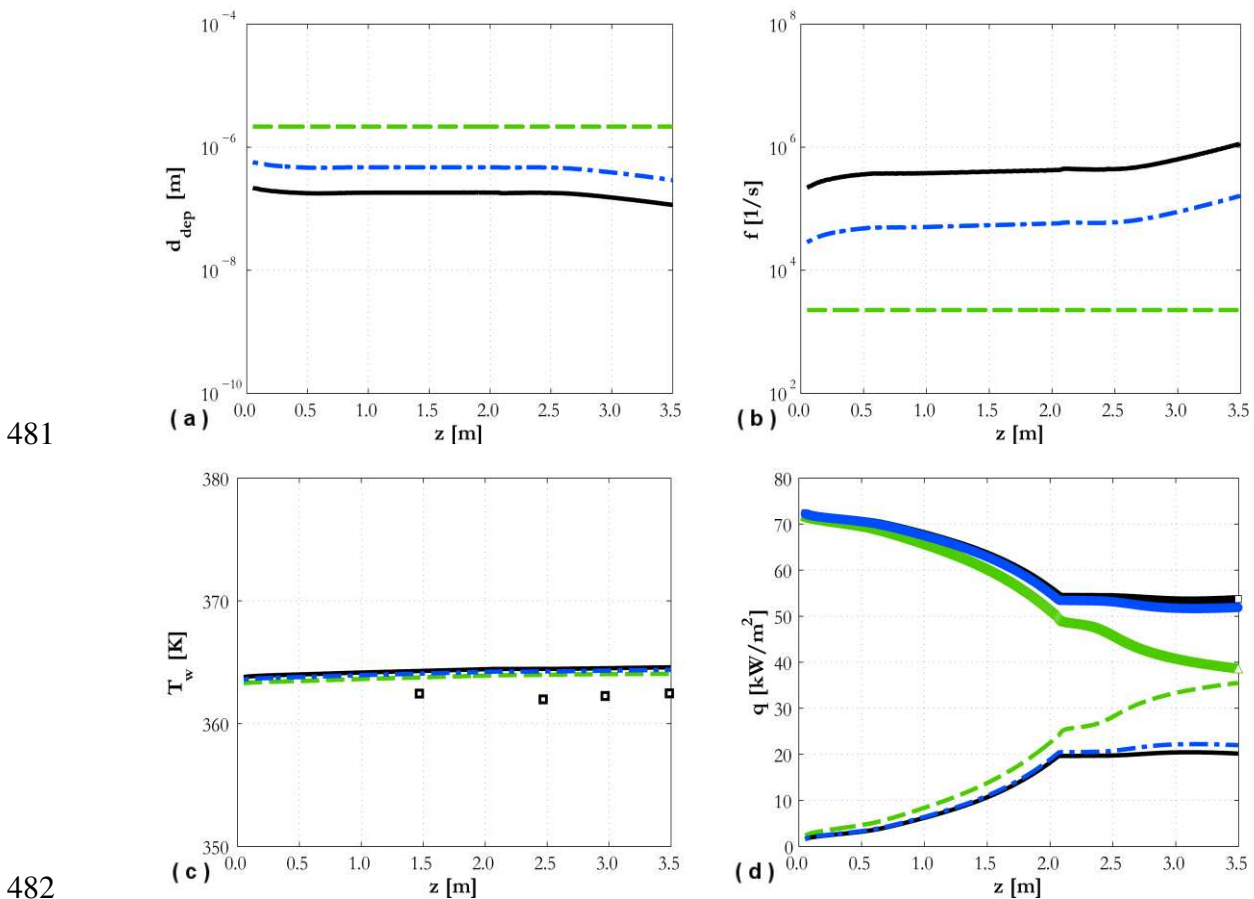
472

Figure 6. Predicted bubble departure diameter (a), bubble departure frequency (b), wall temperature (c) and evaporative and single-phase liquid heat fluxes (d) for Bartolomei and Chanturiya (1967) experiment: (\square) data; ($- -$) Kocamustafaogullari (1983); ($-$) Sugrue and Buongiorno (2016); ($- \cdot -$) Yun et al. (2012) neglecting subcooling. In (d) lines are evaporative and symbols single-phase liquid heat fluxes: (Δ) Kocamustafaogullari (1983); (\square) Sugrue and Buongiorno (2016); (\circ) Yun et al. (2012).

An interesting trend is found in the evaporative heat flux behaviour (Figures 6(d) and 7(d)).

Using the Kocamustafaogullari (1983) correlation, although the departure diameter and frequency are constant along the pipe, the evaporative heat flux increases in the outlet region, possibly because of an increase in the active nucleation site density. In contrast, the evaporative heat flux is much flatter for the two force balance models. In these, a decrease in departure diameter triggers an increase in frequency. Bubble growth is, however, modelled as only 20% of the total ebullition cycle and, therefore, the contribution of the higher departure frequency to the evaporative contribution is weakened. Therefore, further study in this area and more advanced modelling of the total ebullition cycle would be beneficial. Figures 6d and 7d also show the heat

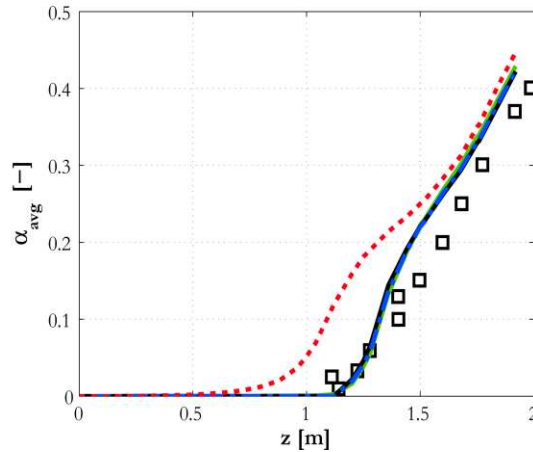
473 flux to the liquid phase. This includes both the convective single-phase and quenching
 474 components of the heat flux partitioning balance. Since a constant heat flux from the wall is
 475 applied in both experiments, an increased heat flux to the liquid phase corresponds to the reduced
 476 evaporative heat flux observed with the Sugrue and Buongiorno (2016) and Yun et al. (2012)
 477 models with respect to the Kocamustafaogullari (1983) approach. To accommodate this greater
 478 heat flux to the liquid phase, both the Sugrue and Buongiorno (2016) and Yun et al. (2012)
 479 models also predict a higher wall temperature.
 480



482
 483 Figure 7. Predicted bubble departure diameter (a), bubble departure frequency (b), wall
 484 temperature (c) and evaporative and single-phase liquid heat fluxes (d) for DEBORA experiment
 485 (Garnier et al., 2001): (\square) data; (---) Kocamustafaogullari (1983); (—) Sugrue and Buongiorno
 486 (2016); (- · -) Yun et al. (2012) neglecting subcooling. In (d) lines are evaporative and symbols
 487 single-phase liquid heat fluxes: (Δ) Kocamustafaogullari (1983); (\square) Sugrue and Buongiorno
 488 (2016); (\circ) Yun et al. (2012).
 489

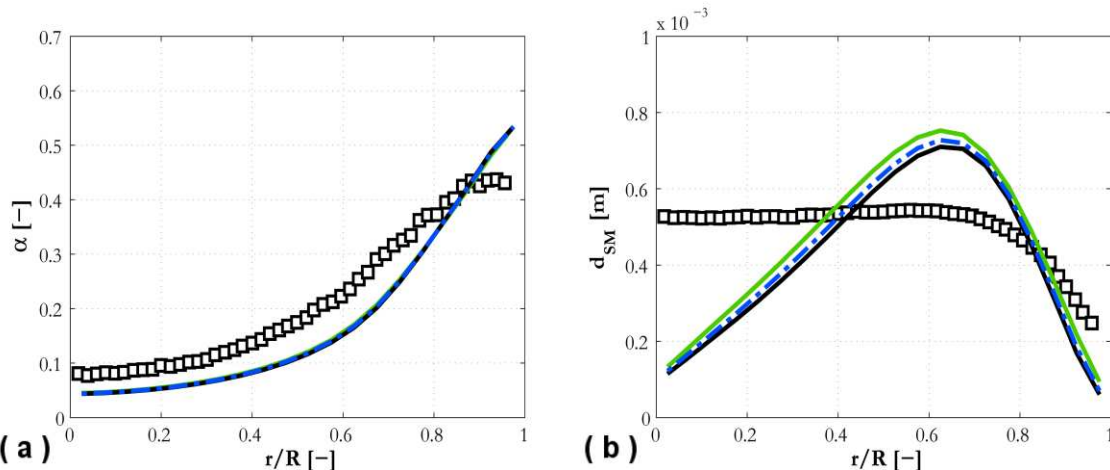
490 Whereas Figure 6 and 7 were focused on wall-related quantities, comparisons for the bulk of the
 491 flow are provided in Figure 8 and 9. Figure 8 shows the average void fraction along the pipe for

492 Bartolomei and Chanturiya (1967). The void increase along the pipe is well-predicted with the
493 Sugrue and Buongiorno (2016), Yun et al. (2012) and Kocamustafaogullari (1983) models. In
494 Figure 8, the model of Tolubinsky and Kostanchuck (1970) is also considered to show how an
495 erroneous value of the bubble departure diameter can negatively affect the value of the void
496 fraction. Specifically, the overestimated (Figure 2a) bubble departure diameter produces an
497 excessive evaporative heat flux component. This causes the overestimation of the amount of void
498 generated at the wall (Figure 8) and the underestimation of the wall temperature, since a reduced
499 amount of heat needs to be accommodated by the liquid phase (Figure 2b). Comparisons against
500 the void fraction and average bubble diameter radial profiles for the DEBORA experiments are
501 provided in Figure 9. The wall-peaked character of the radial void fraction profile is well-
502 predicted (Figure 9a). This further confirms the accurate void prediction from the force balance
503 models in the Bartolomei and Chanturiya (1967) experiment (Figure 8). More discrepancies are
504 found in the average bubble diameter profile (Figure 9b). The increase in diameter away from the
505 wall is well-predicted only for a portion of the radial length. Near the centre of the pipe, all the
506 models predict a significant dip in the diameter, while the experimental profile remains flat.
507 Similar difficulties in predicting the average bubble diameter from the DEBORA experiment
508 were also reported in a previous paper (Colombo and Fairweather, 2016a). These results
509 confirm that additional developments are required in the population balance model that is
510 coupled with the boiling model. In the near wall region, all models underestimate the average
511 diameter. However, the measurements cannot be reliably used to evaluate the accuracy of the
512 bubble departure model. In the experiment, the bubble diameter was measured in the flow and
513 starting from a certain distance from the wall. Even with this distance being only a fraction of a
514 millimeter, bubble diameter at departure is still much smaller in the conditions of the experiment.
515 Therefore, the measurements in these locations were probably already affected by interactions
516 between the bubbles that increased the average bubble diameter but are not entirely accounted
517 for in the overall model.



518
519
520
521
522

Figure 8. Area-averaged void fraction profile along the pipe in Bartolomei and Chanturiya (1967) compared against: (---) Kocamustafaogullari (1983); (—) Sugrue and Buongiorno (2016); (- · -) Yun et al. (2012); (···) Tolubinsky and Kostanchuck (1970).



523
524
525
526
527

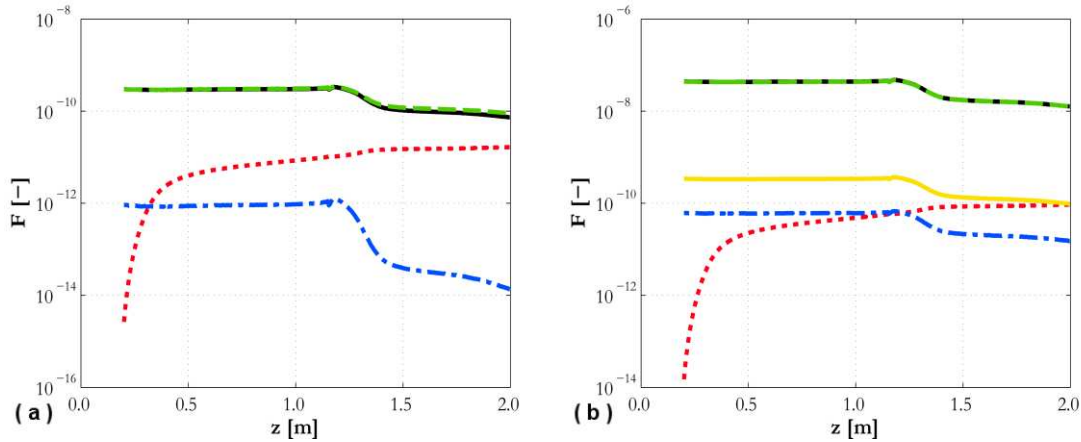
Figure 9. Void fraction (a) and averaged mean diameter (b) radial profiles from the DEBORA experiment compared against: (---) Kocamustafaogullari (1983); (—) Sugrue and Buongiorno (2016); (- · -) Yun et al. (2012).

528
529
530
531
532
533
534
535

Details of the magnitude of each force acting on a bubble can be found in Figures 10 and 11. In both experiments, the surface tension is the dominant force that keeps bubbles attached to the wall, whereas drag parallel to the wall and shear lift perpendicular to the wall promote bubble departure. Other forces are not expected to be significant, including, at these pressures, gravity. Figures 10 and 11 help to explain some of the behaviour observed previously. The magnitude of the surface tension, which is the dominant negative contribution, depends on the value of the contact diameter d_w . From Table 2, Yun at al. (2012) predicts a higher contact diameter than Sugrue and Buongiorno (2016) and, therefore, always a slightly higher bubble departure

536 diameter in Figure 6(a) and 7(a). Klausner et al. (1993), in contrast, gives a constant value that
 537 provides results which are much higher than both of the previous models.

538



539

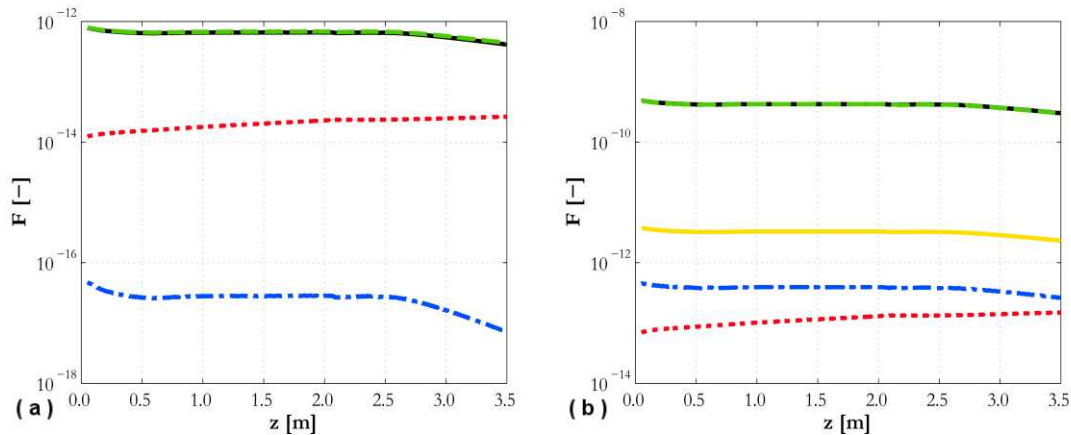
540

541

542

543

Figure 10. Contribution to force balance in wall-parallel (a) and wall-normal (b) directions for Bartolomei and Chanturiya (1967): (—) F_{st} ; (---) F_{qsd} (a) and F_{sl} (b); (···) F_{du} ; (- · -) F_b (a) and F_p (b); (—) F_{cp} .



544

545

546

547

548

549

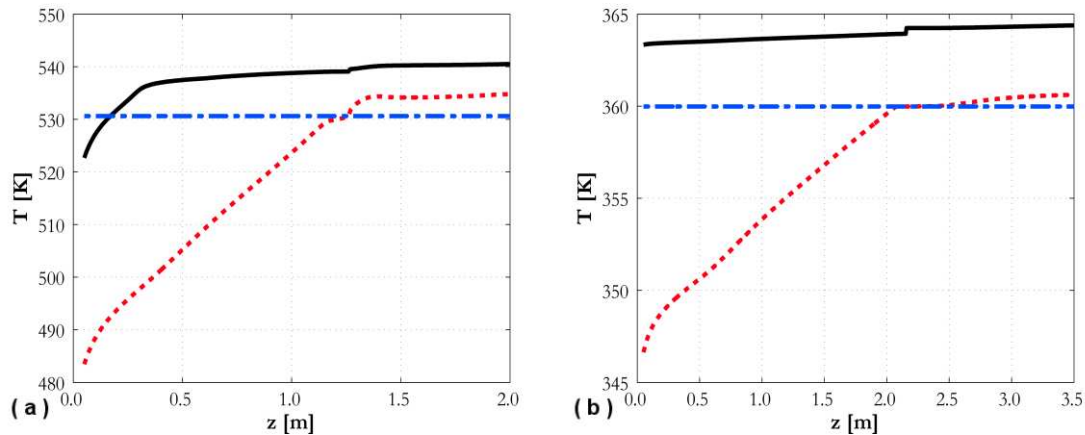
Figure 11. Contribution to force balance in wall-parallel (a) and wall-normal (b) directions for DEBORA experiment (Garnier et al., 2001): (—) F_{st} ; (---) F_{qsd} (a) and F_{sl} (b); (···) F_{du} ; (- · -) F_b (a) and F_p (b); (—) F_{cp} .

549 Therefore, and because of the higher surface tension force, when a solution is reached, the
 550 bubble departure diameter from Klausner et al. (1993) is significantly higher than that of Yun et
 551 al. (2012) and Sugrue and Buongiorno (2016). The latter also both predict a decrease of the
 552 departure diameter near the pipe end. An increase in velocity promoted by boiling is expected to
 553 increase the effect of drag and lift, which are the main forces promoting bubble departure. In
 554 both cases, bubble departure is predicted before lift-off. However, due to uncertainties in the

555 formulation of the drag and lift forces, and in their applicability to the present conditions,
556 additional studies are required.

557
558 Preliminary results obtained with subcooling in the Yun et al. (2012) model are considered in
559 Figure 12, which shows the axial wall temperature distribution. In the majority of the region
560 affected by boiling, the liquid in the first cell is superheated. In the first half of the pipe,
561 however, subcooling is significant. Therefore, when the temperature in the first cell is used to
562 evaluate local subcooling, the condensation rate can become so high that a negative bubble
563 diameter is predicted, thus preventing an acceptable solution from being reached. This is due to
564 the use of the temperature in the centre of the near-wall cell, which must be located some
565 distance from the wall. At the pressures of the experiments, the bubbles are much smaller than
566 the near wall cell size, and the temperature in the first cell is not representative of conditions at
567 the bubble cap. Better quantification of the local value of the temperature on the bubble cap is
568 necessary to account properly for the impact of condensation on bubble departure inside CFD
569 codes.

570



571
572 Figure 12. Predicted temperatures in near-wall region for Bartolomei and Chanturiya (1967) (a)
573 and DEBORA (Garnier et al., 2001) (b): (—) wall temperature; (···) liquid temperature in near-
574 wall cell; (- · -) saturation temperature.

575

576 5. CONCLUSIONS

577

578 Three semi-mechanistic models of bubble departure diameter were implemented into the RPI
579 wall heat flux partitioning model in the STAR-CCM+ code. Model predictions were compared
580 against vertically upward subcooled boiling flows of water and refrigerant. The limited
581 applicability of the model proposed by Klausner et al. (1993), which uses a constant contact

582 diameter in the surface tension force, was demonstrated, and the models of Yun et al. (2012) and
583 Sugrue and Buongiorno (2016), where the contact diameter is a fraction of the bubble diameter,
584 were shown to be preferable. With these two models, the importance of a coupled calculation of
585 the bubble departure diameter and frequency for improved predictions and better physical
586 consistency of the boiling model was demonstrated. Given the similar predictions of these two
587 models, both of which are in reasonable agreement with wall temperature and void fraction
588 measurements, no clear distinction between the two can be made based on the conditions studied
589 in this work. On one hand, Yun et al. (2012) has the advantage of accounting for the impact of
590 subcooling on bubble growth, which may become dominant in some flow conditions. On the
591 other hand, the much more extended validation of the Sugrue and Buongiorno (2016) model
592 makes it more robust. More specifically, Yun et al. (2012) validated their model against the
593 DEBORA experiment, whereas Sugrue and Buongiorno (2016) compared against five different
594 databases and a wide range of fluids, geometries and operating conditions. In addition, the
595 subcooling contribution introduced by Yun et al. (2012) is in need of further improvement.
596 Specifically, excessive condensation resulting in a negative bubble diameter was frequently
597 predicted, because the liquid temperature in the near-wall computational cell was not
598 representative of the local conditions on the bubble cap. Numerous areas for further
599 improvement have been identified. The models predict bubble sliding before lift-off, but the
600 sizes of the surface tension, drag and lift forces, which dominate the force balance, are still
601 uncertain. The general applicability of the models to wall boiling conditions therefore needs to
602 be investigated further. Bubble growth is only a limited part of the whole ebullition cycle and
603 advances in the modelling of the whole cycle, including the contribution of quenching to the total
604 heat flux, are required for more accurate prediction of the bubble departure frequency. Extension
605 of the model from isolated bubble growth to more sustained boiling conditions, including bubble
606 merging and coalescence during growth, is also of interest. Finally, grid-independent methods to
607 predict real local conditions on the bubble cap are required to account for condensation, and
608 these need to be tested in conditions where condensation is expected to be relevant, such as at
609 lower pressures.

610
611
612

613 **ACKNOWLEDGMENTS**

614
615 The authors gratefully acknowledge discussions with Dr. Andrew Splawski and Dr. Simon Lo of
616 CD-adapco and the financial support of the EPSRC, in the framework of the UK-India Civil
617 Nuclear Collaboration through grant EP/K007777/1, Thermal Hydraulics for Boiling and Passive
618 Systems, and EP/M018733/1, Grace Time, and Rolls-Royce plc.

619
620 **NOMENCLATURE**

621

622	A_b	fraction of the wall surface affected by wall boiling [-]
623	a	thermal diffusivity [$\text{m}^2 \text{s}^{-1}$]
624	a_i	interfacial area concentration [$\text{m}^2 \text{m}^{-3}$]
625	C_p	specific heat at constant pressure [$\text{J kg}^{-1} \text{K}^{-1}$]
626	D	pipe diameter [m]
627	d_B	bubble diameter [m]
628	d_{dep}	bubble departure diameter [m]
629	d_{SM}	Sauter-mean bubble diameter [m]
630	d_w	contact diameter [m]
631	F	force [N]
632	f	bubble departure frequency [s^{-1}]
633	G	mass flux [$\text{kg m}^{-2} \text{s}^{-1}$]
634	G_s	dimensionless shear rate [-]
635	g	gravitational acceleration [m s^{-2}]
636	h	heat transfer coefficient [$\text{W m}^{-2} \text{K}^{-1}$]
637	i_{lv}	latent heat of vaporization [J kg^{-1}]
638	Ja	Jacob number [-]
639	K_{dry}	fraction of wall surface in contact with the vapour phase during boiling [-]
640	k	turbulence kinetic energy [$\text{m}^2 \text{s}^{-2}$]
641	L	pipe length [m]
642	M_γ	γ -th moment of the bubble diameter distribution [m^γ]
643	N_A	active nucleation site density [m^{-2}]
644	n	bubble concentration [m^{-3}]
645	p	pressure [Pa]
646	q	thermal flux [W m^{-2}]
647	R	bubble radius [m]
648	Re	bubble Reynolds number [-]
649	S_γ	γ -th moment of the bubble diameter distribution per cubic metre [$\text{m}^\gamma \text{m}^{-3}$]
650	T	temperature [K]
651	T^+	non-dimensional temperature
652	t	time [s]
653	t_w	waiting time [s]
654	U	velocity [m s^{-1}]
655	u_τ	shear velocity [m s^{-1}]
656	We_{cr}	critical Weber number [-]

657	x, y	spatial coordinates [m]
658	y^+	dimensionless wall distance [-]
659	z	pipe axial coordinate [m]
660		
661	<i>Greek symbols</i>	
662	α	void fraction [-]
663	α_i	advancing contact angle [rad]
664	β_i	receding contact angle [rad]
665	γ	bubble inclination angle [rad]
666	ε	turbulence kinetic energy dissipation rate [$\text{m}^2 \text{s}^{-3}$]
667	θ	heated surface inclination angle [rad]
668	λ	thermal conductivity [$\text{W m}^{-1} \text{K}^{-1}$]
669	ν	kinematic viscosity [$\text{m}^2 \text{s}^{-1}$]
670	ρ	density [kg m^{-3}]
671	σ	surface tension [N m^{-1}]
672		

673 ***Subscripts***

674	b	buoyancy
675	br	breakup
676	cl	coalescence
677	cp	contact pressure
678	du	unsteady drag
679	in	inlet
680	l	liquid
681	p	pressure
682	q	quenching
683	qsd	quasi-steady drag
684	sl	shear lift
685	st	surface tension
686	v	vapour
687	w	wall
688		

689 **ACRONYMS**

690	CFD	Computational Fluid Dynamics
691	DNB	Departure from Nucleate Boiling
692	PWR	Pressurized Water Reactor
693	RPI	Rensselaer Polytechnic Institute
694	SMD	Sauter-Mean Diameter
695		

696 **REFERENCES**

697

698 Bartolomei, G.G., Chanturiya, V.M., 1967. Experimental study of true void fraction when boiling
699 subcooled water in vertical tubes. *Thermal Engineering* 14, 123-128.

700 Bestion, D., 2012. Applicability of two-phase CFD to nuclear reactor thermalhydraulics and
701 elaboration of Best Practice Guidelines. *Nuclear Engineering and Design* 253, 311-321.

702 Burns, A.D., Frank, T., Hamill, I., Shi, J.M., 2004. The Favre averaged drag model for turbulent
703 dispersion in Eulerian multi-phase flows. 5th International Conference on Multiphase Flows,
704 Yokohama, Japan, May 30 - June 4.

705 CD-adapco, 2016. STAR-CCM+[®] Version 10.04 User Guide.

706 Cheung, S.C.P., Vahaji, S., Yeoh, G.H., Tu, J.Y., 2014. Modeling subcooled flow boiling in vertical
707 channels at low pressures - Part 1: Assessment of empirical correlations. *International Journal*
708 *of Heat and Mass Transfer* 75, 736-753.

709 Cole, R., 1960. A photographic study of pool boiling in the region of the critical heat flux. *AICHE*
710 *Journal* 6, 533-538.

711 Colombo, M., Fairweather, M., 2015. Prediction of bubble departure in forced convection boiling:
712 A mechanistic model. *International Journal of Heat and Mass Transfer* 85, 135-146.

713 Colombo, M., Fairweather, M., 2016a. Accuracy of Eulerian-Eulerian, two-fluid CFD boiling
714 models of subcooled boiling flows. *International Journal of Heat and Mass Transfer* 103, 28-
715 44.

716 Colombo, M., Fairweather, M., 2016b. RANS simulation of bubble coalescence and break-up in
717 bubbly two-phase flows. *Chemical Engineering Science* 146, 207-225.

718 Cooper, M.G., Lloyd, A.J.P., 1969. The microlayer in nucleate pool boiling. *International Journal*
719 *of Heat and Mass Transfer* 12, 895-913.

720 Del Valle, V.H., Kenning, D.B.R., 1985. Subcooled flow boiling at high heat flux. *International*
721 *Journal of Heat and Mass Transfer* 28, 1907-1920.

722 Forster, H.K., Zuber, N., 1954. Growth of a vapor bubble in a superheated liquid. *Journal of*
723 *Applied Physics* 25, 474-478.

724 Garnier, G., Manon, E., Cubizolles, G., 2001. Local measurements of flow boiling of refrigerant
725 12 in a vertical tube. *Multiphase Science and Technology* 13, 1-111.

726 Gilman, L., Baglietto, E., 2017. A self-consistent, physics-based boiling heat transfer modeling
727 framework for use in computational fluid dynamics. *International Journal of Multiphase Flow*
728 95, 35-53.

729 Hibiki, T., Ishii, M., 2006. Active nucleation site density in boiling systems. *International Journal*
730 *of Heat and Mass Transfer* 46, 2587-2601.

731 Ishii, M., Hibiki, T., 2006. *Thermo-fluid dynamics of two-phase flow*. Springer, New York, USA.

732 Jones, W.P., Launder, B.E., 1972. The prediction of laminarization with a two-equation model of
733 turbulence. *International Journal of Heat and Mass Transfer* 15, 301-314.

734 Klausner, J.F., Mei, R., Bernhard, D.M., Zeng, L.Z., 1993. Vapor bubble departure in forced
735 convection boiling. *International Journal of Heat and Mass Transfer* 36, 651-662.

736 Kocamustafaogullari, G., 1983. Pressure dependence of bubble departure diameter for water.
737 *International Communications in Heat and Mass Transfer* 10, 501-509.

738 Koncar, B., Matkovic, M., 2012. Simulation of turbulent boiling flow in a vertical rectangular
739 channel with one heated wall. *Nuclear Engineering and Design* 245, 131-139.

740 Krepper, E., Rzehak, R., 2011. CFD for subcooled flow boiling: Simulation of DEBORA
741 experiment *Nuclear Engineering and Design* 241, 3851-3866.

742 Krepper, E., Rzehak, R., Lifante, C., Frank, T., 2013. CFD for subcooled flow boiling: coupling
743 wall boiling and population balance models. *Nuclear Engineering and Design* 255, 330-346.

744 Kurul, N., Podowski, M.Z., 1990. Multi-dimensional effects in sub-cooled boiling. 9th
745 *International Heat Transfer Conference*, Jerusalem, Israel, August 19-24.

746 Lo, S., Zhang, D., 2009. Modelling of break-up and coalescence in bubbly two-phase flows.
747 *Journal of Computational Multiphase Flow* 1, 23-38.

748 Mazzocco, T., Ambrosini, W., Kommajosyula, R., Baglietto, E., 2018. A reassessed model for
749 mechanistic prediction of bubble departure and lift off diameters. *International Journal of Heat*
750 *and Mass Transfer* 117, 119-124.

751 Mikic, B.B., Rohsenow, W.M., 1969. A new correlation of pool-boiling data including the effect
752 of heating surface characteristics. *International Journal of Heat and Mass Transfer* 91, 245-250.

753 Plesset, M.S., Zwick, S.A., 1954. The growth of vapor bubbles in superheated liquids. *Journal of*
754 *Applied Physics* 25, 493-500.

755 Ranz, W.E., Marshall, W.R., 1952. Evaporation from drops. *Chemical Engineering Progress* 48,
756 141-146.

757 Situ, R., Hibiki, T., Ishii, M., Mori, M., 2005. Bubble lift-off size in forced convective subcooled
758 boiling flow. *International Journal of Heat and Mass Transfer* 48, 5536-5548.

759 Sugrue, R., Buongiorno, J., 2016. A modified force-balance model for prediction of bubble
760 departure diameter in subcooled flow boiling. *Nuclear Engineering and Design* 305, 717-722.

761 Thakrar, R., Murallidharan, J., Walker, S.P., 2014. An evaluation of the RPI model for the
762 prediction of the wall heat flux partitioning in subcooled boiling flows. 22nd International
763 Conference on Nuclear Engineering (ICONE-22), Prague, Czech Republic, July 7-11.

764 Thakrar, R., Murallidharan, J., Walker, S.P., 2017. CFD investigation of nucleate boiling in non-
765 circular geometries at high pressure. *Nuclear Engineering and Design* 312, 410-421.

766 Thakrar, R., Walker, S.P., 2016. CFD prediction of subcooled boiling flow with semi-mechanistic
767 bubble departure diameter modelling. 25th International Conference Nuclear Energy for New
768 Europe (NENE-2016), Portoroz, Slovenia, September 5-8.

769 Tolubinsky, V.I., Kostanchuk, D.M., 1970. Vapour bubbles growth rate and heat transfer intensity
770 at subcooled water boiling 4th International Heat Transfer Conference, Paris, France.

771 Tomiyama, A., Kataoka, I., Zun, I., Sakaguchi, T., 1998. Drag coefficients of single bubbles under
772 normal and micro gravity conditions. *JSME International Journal Series B Fluids and Thermal*
773 *Engineering* 41, 472-479.

774 Wu, W., Chen, P., Jones, B.G., Newell, T.A., 2008. A study of bubble detachment and the impact
775 of the heated surface structure in subcooled nucleate boiling flows. *Nuclear Engineering and*
776 *Design* 238, 2693-2698.

777 Yadigaroglu, G., 2014. CMFD and the critical-heat-flux grand challenge in nuclear thermal-
778 hydraulics. *International Journal of Multiphase Flow* 67, 3-12.

779 Yao, W., Morel, C., 2004. Volumetric interfacial area prediction in upward bubbly two-phase flow.
780 *International Journal of Heat and Mass Transfer* 47, 307-328.

781 Yeoh, G.H., Tu, J.Y., 2006. Two-fluid and population balance models for subcooled boiling flow.
782 *Applied Mathematical Modelling* 30, 1370-1391.

783 Yeoh, G.H., Vahaji, S., Cheung, S.C.P., Tu, J.Y., 2014. Modeling subcooled flow boiling in vertical
784 channels at low pressures - Part 2: Evaluation of mechanistic approach. *International Journal of*
785 *Heat and Mass Transfer* 75, 754-768.

786 Yun, B.J., Splawski, A., Lo, S., Song, C.H., 2012. Prediction of a subcooled boiling flow with
787 advanced two-phase flow models. *Nuclear Engineering and Design* 253, 351-359.

788 Zeng, L.Z., Klausner, J.F., Bernhard, D.M., Mei, R., 1993a. A unified model for the prediction of
789 bubble detachment diameters in boiling systems - I. Pool boiling. *International Journal of Heat*
790 *and Mass Transfer* 36, 2261-2270.

791 Zeng, L.Z., Klausner, J.F., Mei, R., 1993b. A unified model for the prediction of bubble detachment
792 diameters in boiling systems- II. Flow boiling. *International Journal of Heat and Mass Transfer*
793 36, 2271-2279.

794